On a Fast Analytical Approximation of Natural Frequencies for Photovoltaic Modules

TECHNISCHE MECHANIK
an open access journal

journal homepage: www.ovgu.de/techmech

Tech. Mech., Vol. 40, Is. 2, (2020), 191–203

Received: 30.07.2019
Accepted: 22.10.2020
Available online: 30.10.2020

On a Fast Analytical Approximation of Natural Frequencies for Photovoltaic Modules

Stefan Bergmann[1], Fereshteh Hassani[2], Zia Javanbakht[3]*, and Marcus Aßmus[1]

[1] Otto von Guericke University, Institute of Mechanics, UniversitÃđtsplatz 2, 39106 Magdeburg, Germany
[2] University of Tabriz, Faculty of Civil Engineering, 29 Bahman Boulevard, Tabriz, Iran
[3] Griffith University, School of Engineering and Build Environment, Parklands Dr, Southport 4215, Australia

Abstract: In this paper, an eigenvalue problem is considered, i.e., the free vibration of photovoltaic (PV) modules. This structure was selected for its peculiar layer contrast, which forms an anti-sandwich. The aim was to present an analytical procedure for obtaining the natural frequencies of the PV modules over a range of temperatures. To this end, the layered structure was homogenised into an equivalent single layer for which a closed-form solution is presented using the shear-rigid plate theory. Moreover, the finite element method was applied to simulate the behaviour of the discrete layers in terms of mesh sensitivity. By examining the findings and some benchmark values, it was found that the analytical procedure could provide a range for the results. More specifically, the Reuss-Voigt range covers the possible values for the natural frequencies in the examined temperature range. Moreover, the analytical method can predict the natural frequencies with a good accurracy in the temperature range of −40 to 15°C. In contrast, the computational analysis seemed to provide very good results in return for a modest computational effort. In conclusion, the provided analytical procedure could quickly determine the natural frequecies with a good accuracy in the mentioned range.

Keywords: composite structure, homogenisation, plate theory, finite element method

1 Introduction

Overview. Composite structures, due to their high specific properties, are used in various applications in which the vibration of components is inevitable. Of our interest is the so-called anti-sandwich panels, which can be categorised under laminated composites. An anti-sandwich consists of two stiff skin layers and a soft core layer (Aßmus, 2019; Javanbakht et al., 2019). This typical structure is used in manufacturing photovoltaic (PV) modules (Aßmus et al., 2016).

Dynamic analysis. The dynamic performance of structures is measured by studying their vibrational behaviour. The inherent dynamic property of a structure reveals itself under initial excitation (free vibration). The behaviour of the system in this state depends on the natural frequencies of the system, which is obtained from a modal analysis. This information is used to investigate more complex responses, e.g., forced excitation (cyclic/harmonic loads) or transient analysis (damped system under impact) (Meirovitch, 2001).

Damage control/detection. The results of the dynamic analyses can be used in either *damage control* or *damage detection* in PV modules. In the former case, the information is used for fine-tuning the geometric and material parameters during the design process in order to restrict the dynamic response. In the latter context, studying the dynamic behaviour could reveal the extent of damage in the PV modules. For instance, the resonance ultrasonic vibrations method is used as a non-destructive test to detect microcracks (Dallas et al., 2007). In terms of damage control, both *structural* and *functional* failure modes are possible, and thus are required to be covered in the investigations.

Structural failure. Structural damage could happen under either static or dynamic loading. Photovoltaic modules experience most of the static loads during operation; a general solution for arbitrary loading condition is presented in (Aßmus et al., 2017a). More broadly, the dynamic response of the PV modules becomes significant under both pre-operating conditions (transportation-induced vibrations during shipping (Reil et al., 2010) or during installation) and under service (vortex shedding from wind impact (Aßmus and Köhl, 2012)); experimental studies have shown that resonance could occur in such conditions (Aßmus et al., 2011) and cause failure in the module.

Functional failure. Dynamic loads could damage the functionality of the electrical components in PV modules, e.g., broken interconnect ribbons, solar cell fracture or solder bond failure are possible, see (Ferrara and Philipp, 2012; Köntges et al., 2014; Wohlgemuth, 2020) for various failure modes of this type. It seems that dynamic loads cause more functional damage than

* E-mail address: zia.javanbakht@gmail.com
doi: 10.24352/UB.OVGU-2020-025

structural. For instance, a higher failure rate of the electrical circuits was reported under dynamic loads due to the loss of solder contact (Koch et al., 2010).

Design requirements. The dynamic response of PV modules should be improved to alleviate any harmful stimuli. This is done by some design alterations, which could provide some additional protection against vibration. For example, it was shown that using silicone encapsulants, instead of ethylene vinyl acetate (EVA) copolymer, could better protect the solar cells under dynamic loads (Mickiewicz et al., 2011). Therefore, standardised approaches are emerging in the literature to address the design requirements.

Current standardised approach. The International Electrotechnical Commission (IEC) imposes the minimum design requirements on the PV modules that are manufactured in Europe—the UK implementation of these are published in British Standards. The British code for terrestrial PV modules—BS EN 61215-1-2:2017 (equivalent to IEC 61215) (British Standards, 2017a) and BS EN 61215-2-2017 (British Standards, 2017b) for crystalline silicon modules, and BS-EN-61646:2008 (equivalent to IEC 61646) (British Standards, 2008) for thin-film modules—only demand a static load testing (uniform load) and a hail test (spherical ice ball impact) as minimum design qualifications. Nevertheless, more attention was directed towards the dynamic properties of the PV modules and their regularisation in the recent years. For example, the transportation testing procedure of IEC 62759:2015 (British Standards, 2015) demands a dynamic loading test according to IEC 62782:2016 (British Standards, 2016) along with humidity freeze and thermal cycling. As the first step, the regulated design requirements are indispensable. However, the behaviour of PV modules should be further understood—especially under unconventional circumstances. To this end, a combination of analytical, numerical, and experimental methods are used.

Experimental efforts. In terms of physical experiments, natural frequencies are obtained under various conditions. An outdoor setup was used in (Weiss et al., 2009) where the deflection of a panel was monitored under wind excitation. Fundamental frequency of 9 and 12 Hz was obtained by means of Fourier Transformation. Moreover, an indoor acoustic test resulted in the range of 14.6–24.6 Hz for the natural frequencies of various PV modules including the outdoor test sample. It seemed that the acoustic test provided more consistent results. A similar attempt was made in (Aßmus et al., 2011) where by combining experiments and finite element (FE) simulations, a range of 14.7–27.2 was reported for the fundamental frequency of various PV modules. In (Pingel et al., 2009), the shaking table test was used to simulate the vibrations during transportation (5–500 Hz); it resulted in a resonance frequency in the range of 1–15 Hz. It was also shown that reducing the wafer thickness would increase the failure rate of the PV modules under dynamic loads. In (Kilikeviciene et al., 2019), it was experimentally shown that the impact of hail could cause microcracking in PV modules and render them ineffective in terms of power generation. An experimental setup for harsh weather conditions was introduced in (Visniakov et al., 2015), which considered induced frequencies up to 40 Hz; it was found that the low frequency loads, which represent windy conditions, could cause damage to the crystalline structure of the PV cells and reduce the performance of the modules. Therein, a fundamental frequency of 7.2 Hz was obtained experimentally while the FE simulation resulted in 6.69 Hz. In (Kilikevicius et al., 2016), a similar setup was use to carry out an *operational modal analysis*, which resulted in a fundamental frequency of about 16 Hz. In this study, it was again affirmed that low-frequency studies could be used to simulate the excitations due to various wind speeds. Moreover, the damping characteristics of the PV modules were considered in the experiments. It is worth mentioning that the variation in the geometry and material property of the PV modules as well as the environmental parameters has resulted in a rather wide range of reported frequencies in the literature.

Computational efforts. The experimental efforts are valuable and necessary but they cannot cover all the possible cases; moreover, they are expensive and time-consuming. Computational methods could, at least partially, reduce such costs—especially when combined with analytical methods. For instance, FE analyses were carried out to obtain the mechanical/thermo-mechanical response (Dietrich et al., 2010; Aßmus et al., 2011; Sander et al., 2013; Beinert et al., 2019) of PV modules. The free vibration of PV modules was simulated using the FE method in (Dallas et al., 2007; Visniakov et al., 2015; Kilikevicius et al., 2016). A multi-scale FE analysis was carried out to study the distribution and orientation of microcracking in PV modules. In this study, both of the functional and structural damage of PV modules were considered in coupled elastic-electric analyses. More specialised approaches, such as the extended Layer-Wise Theory (XLWT) (Naumenko and Eremeyev, 2014), are used as the basis of more computationally effective analyses, see (Aßmus et al., 2017b,c).

Aim. All the aforementioned efforts were ideally seeking a balanced approach between complexity and computational cost. Most of the studies were focused on the static loading conditions and the majority of dynamic studies were limited to experimental setups. Herein, the aim is to provide a simple approximation method for the fundamental natural frequency of the PV modules. To this end, an analytical formulation of the homogenised structure is set up and solved. It is hypothesised that the high contrast of material properties might affect the accuracy of the results. Moreover, a computational prototype was developed to complement the study. The current work is restricted to glass-encapsulant-glass structures with structural symmetry in the thickness direction. However, it can be extended to other anti-sandwich structures.

Outline In the following sections, the homogenisation procedure of the PV modules is elaborated. Then, the shear-rigid plate theory is revisited to obtain the closed-form solution for the eigenvalue problem of PV modules. Finally, a computational prototype is analysed in terms of sensitivity of the results to mesh density and temperature change. Then, the results are benchmarked

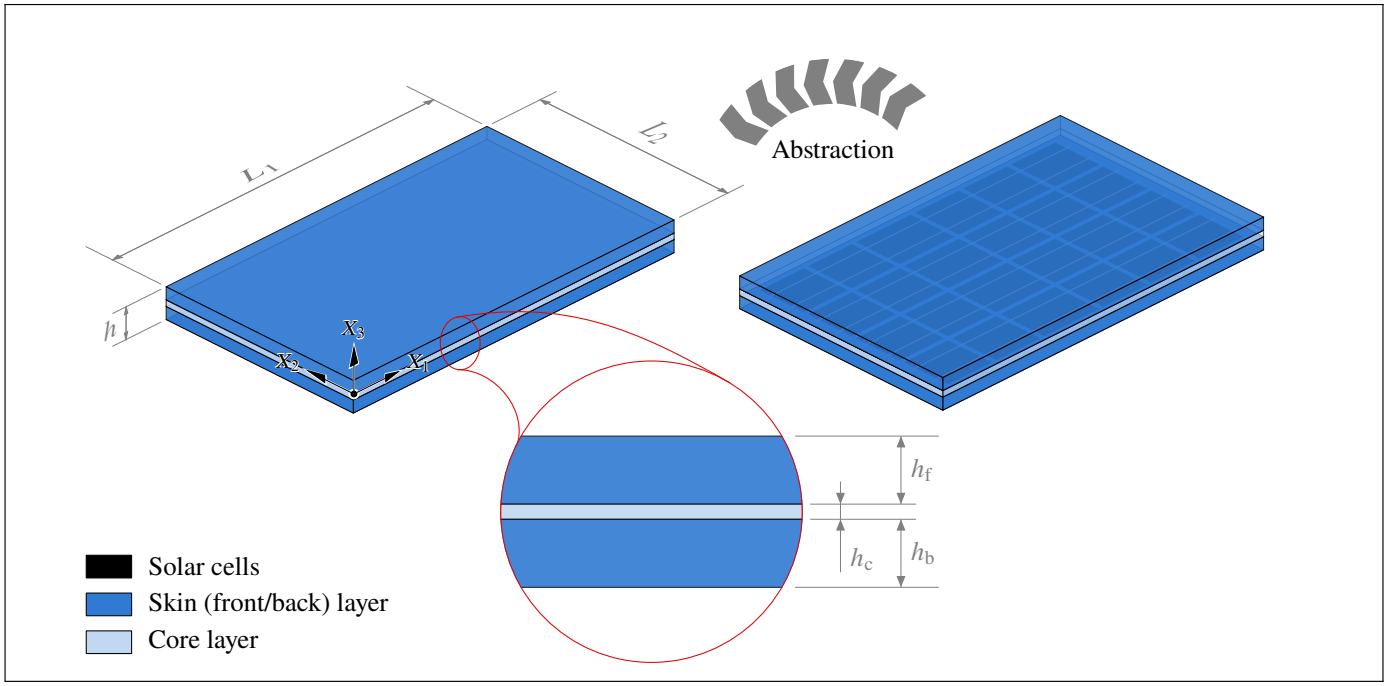

Fig. 1: Abstraction of the geometry and the resulting dimensions for a PV module

against some reported values from the literature and discussed. The final section concludes the findings and suggests some research pathways.

2 Homogenisation of Photovoltaic Modules

2.1 Simplifying the Physical Structure

Geometry. The physical structure of a silicon PV module is illustrated in Fig. 1. Solar cells are embedded in a polymeric core layer, which is covered by front and back skin layers. The contribution of the embedded metallic solar cells to the overall bending and membrane stiffnesses of the laminate can be neglected (Naumenko and Eremeyev, 2014). Thus, a symmetrical anti-sandwich laminate can adequately represent the mechanical behaviour of a PV module. The dimensions of the PV module is $L_1 \times L_2 \times h$ where the overall thickness h is the sum of the thickness of the front (h_f), back (h_b), and core (h_c) layers. In this study, a symmetrical structure is assumed for the PV module whose dimensions are listed in Tab. 1. The front or back layer in a symmetrical photovoltaic module is addressed as a skin layer, e.g., the h_s represents the thickness of the skin ($h_\mathrm{s} = h_\mathrm{f} = h_\mathrm{b}$).

Boundary Conditions. In Fig. 2, the cross-section of a PV module is illustrated. The embedding (often aluminium) frame holds the laminate by a soft sealant. This fixture allows for small rotations, and thus a moment-free constraint can represent this arrangement. Mathematically, this is equivalent to a plate that is simply-supported along the edges:

$$\forall X_1 \in [0, L_1] : \begin{cases} w(X_1, 0) = & w(X_1, L_2) = 0 \\ M_2(X_1, 0) = & M_2(X_1, L_2) = 0 \end{cases}, \tag{1a}$$

$$\forall X_2 \in [0, L_2] : \begin{cases} w(0, X_2) = & w(L_1, X_2) = 0 \\ M_1(0, X_2) = & M_1(L_1, X_2) = 0 \end{cases}, \tag{1b}$$

where w is the deflection (displacement along X_3-axis) of the plate midplane; M_1 and M_2 are the bending moments acting on the planes with normals X_1 and X_2, respectively.

Tab. 1: Geometric parameters

Layer(s)	L_1 [mm]	L_2 [mm]	h_k [mm]
Skin	1620	810	3.2
Core	1620	810	1.0

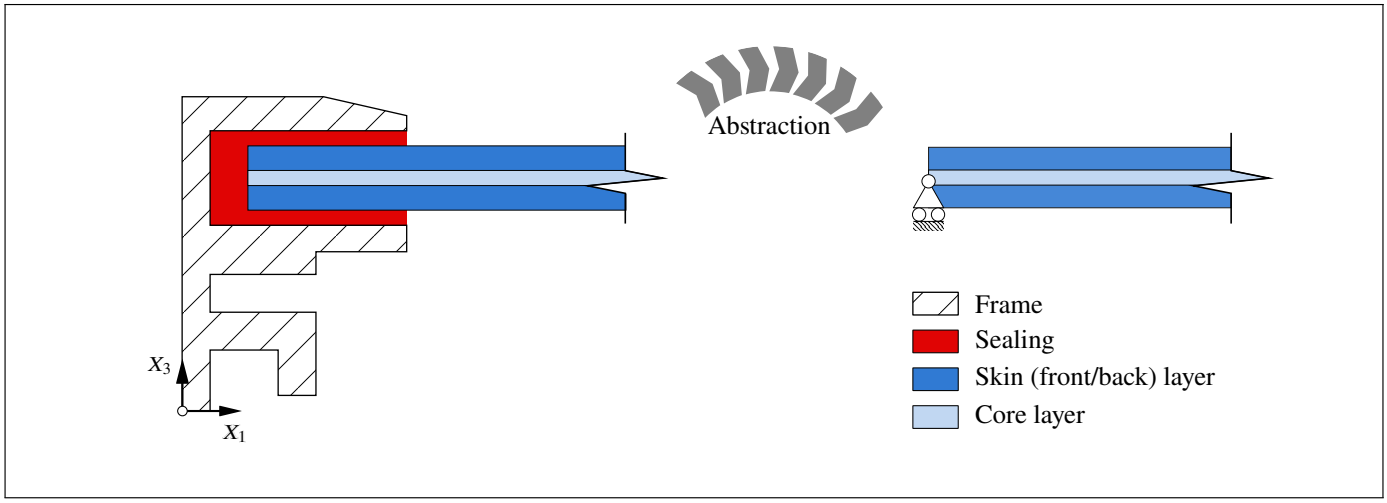

Fig. 2: Cross section view of typical bedding of a PV laminate in a frame and mechanical analogue

2.2 Material Properties

The skin layers of PV modules (front/back layers) are made of glass while the core layer is the EVA polymer, see Tab. 2. The outer layers are denser than the core layer $\rho_s/\rho_c \approx 2.69$ but more importantly, a high contrast of order about $E_s/E_c \approx 10^4$ is observed for their elastic moduli. The Poisson's ratios $\nu_s/\nu_c \approx 0.73$ denotes similar values for the skin and core layers.
BS standards for both crystalline and thin-film modules (British Standards, 2017b, 2008) require thermal cycling from −40 to 85°C for no more than 6 hours. The module temperatures can vary in natural weathering between −20°C (alpine) and +60°C (desert), which is well covered the mentioned range. While the material properties of the skin layers (glass) and the solar cells (polycrystalline silicon) can be deemed temperature-independent, the thermal sensitivity of the polymeric encapsulant cannot be ignored, see (Aßmus et al., 2016).
In the current study, the Poisson's ratio and mass density of the EVA were assumed to be temperature-independent and the respective room temperature properties were used, see Tab. 2. In contrast, the elastic modulus of the EVA is specified as a function of temperature. Using the discrete data that is provided in Tab. 3, the following piecewise linear interpolations were obtained for the elastic modulus of the core layer:

$$E_c(\theta) = \begin{cases} -16.05\theta + 377.046 & \text{for} \quad -40 \le \theta \le 23 \\ -0.12974\theta + 10.8778 & \text{for} \quad 23 \le \theta \le 80 \end{cases}, \tag{2}$$

where θ is the ambient temperature and $E_c(\theta)$ returns the elastic modulus of the core in $^{\mathrm{N}}/_{\mathrm{mm}^2}$, see Fig. 3. It is worth mentioning that increasing the temperature from −40 to +80°C reduces the elastic modulus to 0.05% of its initial value. This reduction happens in a very high rate up to +23°C but after this point, continues with less intensity. Moreover by increasing the temperature, the E_c/E_s ratio approaches zero, and thus the elastic modulus contrast is magnified. For instance, at the highest temperature, the elastic modulus of the skin becomes about $1.4 \cdot 10^5$ times that of the core layer.

2.3 Voigt and Reuss Bounds

The Voigt (Voigt, 1910) and Reuss (Reuss, 1929) bounds are the results of iso-strain and iso-stress assumptions, respectively. It is assumed that various phases of the material undergo the same strain in the former case whereas in the latter case, every phase experiences the same stress, see Fig. 4. In order to simplify the problem, working with a homogeneous medium is preferred. The properties of such smeared continuum is based on its constituents, which are the layers of the PV modules in the current context. The so-called rule of mixture and the inverse rule of mixture (Javanbakht et al., 2020a,b) could be used to obtain various homogenised properties:

$$\square_{\mathrm{V}} = \sum_{i=1}^{n} \zeta^{(i)} \square^{(i)}, \tag{3a}$$

$$\square_{\mathrm{R}} = \left[\sum_{i=1}^{n} \frac{\zeta^{(i)}}{\square^{(i)}} \right]^{-1}, \tag{3b}$$

Tab. 2: Room-temperature material properties

Layer(s)	Material	E_k [$^{\mathrm{N}}/_{\mathrm{mm}^2}$]	ν_k [−]	ρ_k [$^{\mathrm{kg}}/_{\mathrm{m}^3}$]
Skin	Glass	$73 \cdot 10^3$	0.30	2500
Core	EVA	7.90	0.41	930

Tab. 3: Temperature-dependent material parameters of the EVA encapsulant; adapted from (Eitner, 2011)

θ [°C]	−40	+23	+80
E_c [N/mm²]	1019.04	7.90	0.52

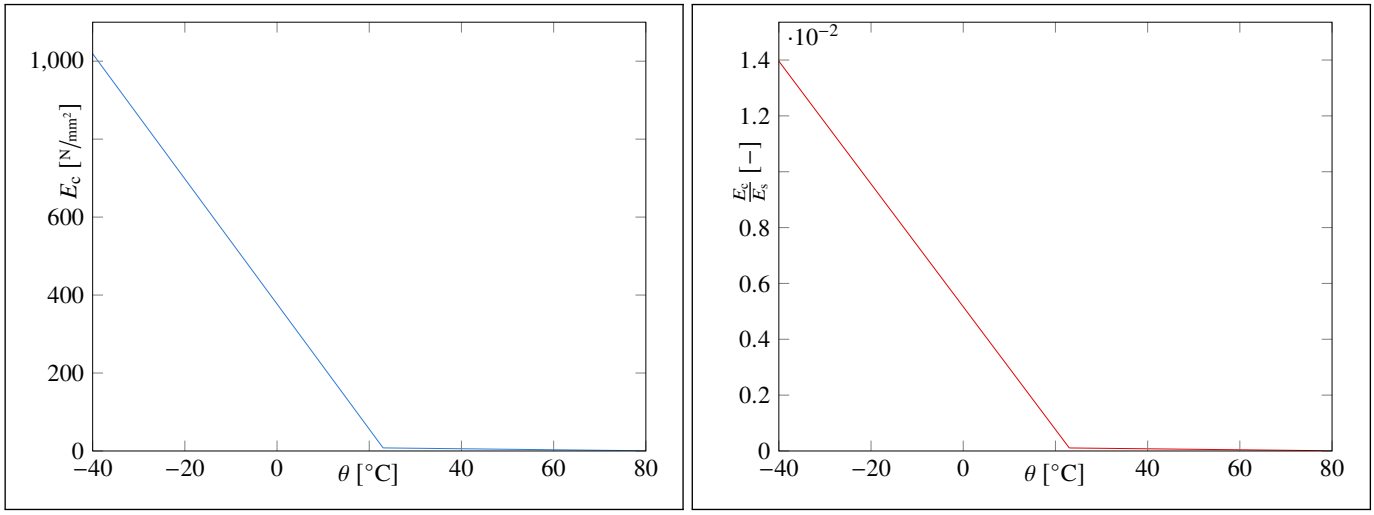

(a) (b)

Fig. 3: Temperature-dependent properties: (a) elastic modulus of the core, and (b) core to skin relative elastic modulus

with $\square \in \{E, \nu, \rho\}$ denotes the material property of interest, and the $(\square_V)$ and $(\square_R)$ subscripts denote the pertaining Voigt and Reuss bounds, respectively; n is the number of phases in the material, $\zeta^{(i)}$ is the volume fraction of the phase, and $\square^{(i)}$ is the material property of the i-th phase.

The Voigt and Reuss bounds respectively represent the upper and lower bounds for the homogenised material properties. In terms of PV modules, these bounds correspond to the direction along the layers (Voigt bound) and the direction perpendicular to the layers (Reuss bound), see Fig. 4. Thus, the homogenisation process replaces the layered structure of the PV modules by an anisotropic homogenised medium. In the following section, the homogenised material properties (elastic modulus, Poisson's ratio, and mass density) are expressed in terms of the layer thicknesses of the PV module.

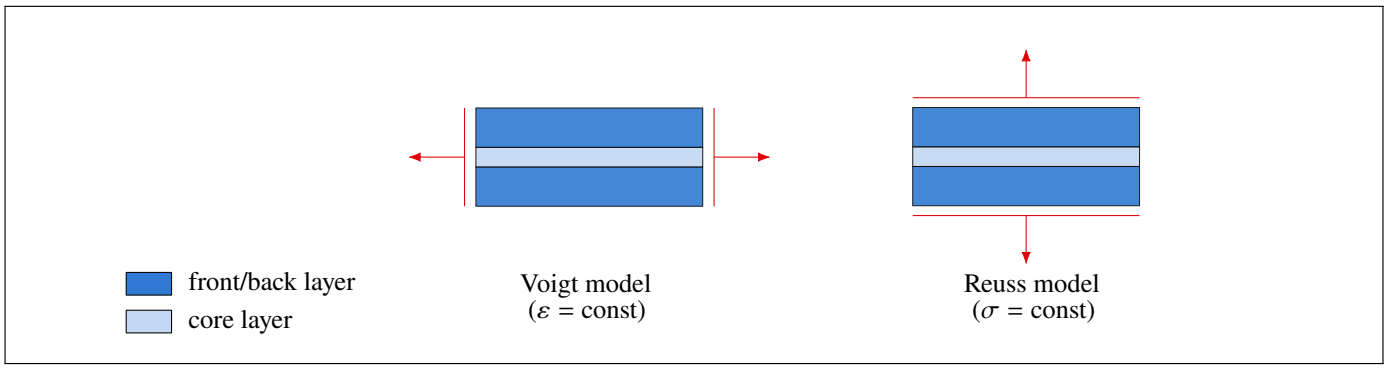

Fig. 4: Underlying assumptions of bounds used for homogenization of photovoltaic composite structure

3 Eigenfrequency Analysis

3.1 Shear-rigid Plate Theory for a Homogenised Medium

Assumptions. In the foregoing section, the effective mechanical properties of a layered structure is obtained as a single equivalent layer. Thereby, instead of any advanced layer-wise theories (Aßmus et al., 2017c; Aßmus, 2019), any single-layer plate theory could be used for determining the natural frequencies. The selection of an appropriate plate theory poses two main considerations:

1. Slenderness hypothesis (with regards to shear rigidity), which decides between a shear-rigid or shear-deformable theories. The thinness of a structural element can be quantitatively measured by defining the slenderness (s) of a body (see Fig. 8):

$$s := \frac{h}{L_{\min}} \qquad \text{with} \quad L_{\min} := \min\{L_1, L_2\} \quad \text{and} \quad h := \sum h_k, \tag{4}$$

which for a shear-rigid theory, is limited to $s < 0.1$ (Altenbach, 2008) or more restrictive values such as $s < 0.05$ (Ugural, 2010). Taking into account the geometric data from Tab. 1, $s \approx 9.25 \cdot 10^{-3}$ results, which underlines the assumption.

2. Geometrical linearity or nonlinearity of the problem; in the former case, the nonlinear geometrical terms are neglected, and thus a zero strain is imposed at the mid-surface (Ugural, 2010). In engineering practice, geometrical linearity is ensured by imposing a limit on the maximum deflection, e.g., deflections smaller than the empirical values of $w_{\max} < 0.5H$ (Birman, 2011) or $w_{\max} < 0.2H$ (Altenbach, 2008). However, a limitation (much smaller than 10°) must be applied to the rotations too (Reddy, 2006), i.e., for a complete linear geometry, small strain and small rotations must be guaranteed.

Considering the thinness of the PV modules and restricting the study to first order deformations, the Kirchhoff-Love plate theory is deemed reasonable. By adopting the engineering approach (as opposed to the direct approach) towards the formulation of such thin walled structures, all considerations are reduced to a reference surface, i.e., the mid-surface. Namely, the assumption of plane stress state degenerates the 3D continuum to a 2D counterpart. In this regard, Kirchhoff-Love hypotheses (Kirchhoff, 1850; Reddy, 2006) are adopted, which assume that the transverse normals

- remain straight after deformation,
- are rigid, and
- remain perpendicular to the mid-surface after deformation.

Herein, the following additional assumptions are made:

- geometrical linearity:
  - infinitesimal cross section rotations, and
  - infinitesimal strains;
- physical linearity: material behaviour is linear elastic;
- material homogeneity: all material points have the same physical properties; and
- material isotropy: there is no preferred direction for physical properties.

Formulation. Considering the aforementioned simplifications, the eigenvalue problem of an isotropic plate is restated for a homogenised medium. In the course of this procedure, an overbar ($\overline{\square}$) denotes the respective effective material property, i.e., it can be either Voigt ($\square_{\mathrm{V}}$) or Reuss ($\square_{\mathrm{R}}$) homogenised values. The governing partial differential equation of thin plates in canonical form is

$$\overline{K}\Delta\Delta w(X_1, X_2, t) + \overline{\rho} h \ddot{w}(X_1, X_2, t) = 0 \qquad \text{with} \quad \overline{K} = \frac{\overline{E} h^3}{12\left(1 - \overline{\nu}^2\right)}, \tag{5}$$

where $\overline{K}$ is the flexural rigidity of the homogenised plate, w is the deflection of the plate midplane, t is time, and ($\Delta := \nabla \cdot \nabla$) is the Laplace operator. First, the Bernoulli approach is used to multiplicatively separate the temporal (T) and spatial (W) components:

$$w(X_1, X_2, t) = W(X_1, X_2)\, T(t), \tag{6}$$

which must satisfy Eq. (5), and thus

$$\Delta\Delta W(X_1, X_2) - \lambda^4 W(X_1, X_2) = 0, \qquad \text{with} \quad \lambda^4 := \frac{\overline{\rho} h \omega^2}{\overline{K}}, \tag{7a}$$

$$\ddot{T}(t) + \omega^2 T(t) = 0, \tag{7b}$$

where ω is the angular frequency of the vibration. Consequently, the oscillation equation takes the following form:

$$\frac{\overline{K}\Delta\Delta W(X_1, X_2)}{\overline{\rho} h W(X_1, X_2)} = -\frac{\ddot{T}(t)}{T(t)} = \omega^2. \tag{8}$$

The time dependency can be represented by the harmonic ansatz $T = A\sin(\omega t + \alpha)$ where α is a constant denoting the phase shift. Consequently, the temporal component of Eq. (6) is obtained:

$$w(X_1, X_2, t) = W(X_1, X_2)\sin(\omega t + \alpha). \tag{9}$$

The spatial component is the solution of the classic Navier problem (a simply supported plate at all edges under a distributed load), i.e, a double Fourier series:

$$W(X_1, X_2) = \sum_{m=1}^{M}\sum_{n=1}^{N} W_{mn} \sin\left(\frac{m\pi}{L_1}\right) X_1 \sin\left(\frac{n\pi}{L_2}\right) X_2, \tag{10}$$

where W_{mn} is the amplitude of the eigenmode shape mn whose magnitude can be scaled arbitrarily; moreover, m and n are the number of mode shape half-waves along the X_1 and X_2 axes, respectively. Finally, substituting this solution into Eq. (7a) results in

$$f_{mn} = \frac{\pi}{2}\left(\frac{m^2}{L_1^2} + \frac{n^2}{L_2^2}\right)\sqrt{\frac{\overline{K}}{\overline{\rho} h}}, \qquad \forall\, m, n = \{1, 2, 3, \dots\}, \tag{11}$$

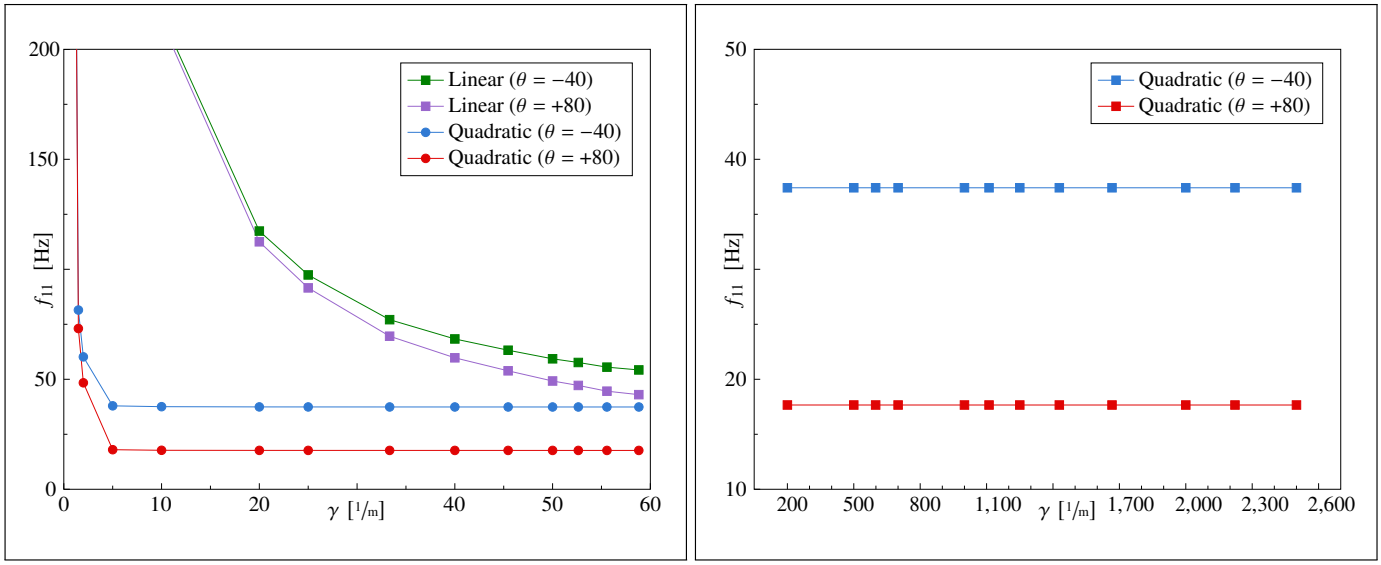

Fig. 5: Convergence study of linear and quadratic elements for two temperature extremes: (a) in-plane mesh sensitivity, and (b) through-thickness mesh sensitivity.

where f_{mn} is the natural frequency of the mode with $m \times n$ half-waves. Note that the angular frequency is related to its linear counterpart (f) via $\omega = 2\pi f$.
In order to compare the results of the closed-form (f_{mn}, $\forall\, m, n \in \{1, 2, 3\}$) and the computational solution (f_i, $\forall\, i \in \{1, \ldots, 9\}$), the pseudo index r is defined as

$$r := \begin{cases} \frac{m \cdot n}{m} + (m-1) & \text{if } m = 1 \\ \frac{m \cdot n}{m} + (m+1) & \text{if } m = 2\,, \\ \frac{m \cdot n}{m} + (m+3) & \text{if } m = 3 \end{cases} \qquad \forall\, n \in \{1, 2, 3\}. \tag{12}$$

The transformation into a sorted sequence f_i follows the $f_i : \; f_r < f_{(r+1)}$ convention.

3.2 Computational Model

A 3D FE model was prototyped using the MSC MARC/MENTAT commercial FE package (Javanbakht and Öchsner, 2017, 2018). A python script was used to populate the models for the convergence and parametric studies. The former provides a nominated model that is used to obtain the natural frequencies in the Results section. Note that the same geometrical parameters and material properties in Tables 1–3 were used. Moreover, the real geometry of the boundary, i.e., the frame, and the solar cells were not considered in the computational models, see Figs. 1 and 2. However, solid elements were used to represent each layer discretely.

Convergence study. In order to remove the sensitivity of the results to the size of elements, the convergence of the fundamental frequency was studies. Since 3D elements were used in the FE prototype, discretisation of the elements in the X_1-X_2 plane (planar), and then along the X_3 axis (through-thickness) was considered. To this end, the planar element mesh density (γ) is defined as (Javanbakht et al., 2017a,b)

$$\gamma := \frac{1}{\ell}, \tag{13}$$

where ℓ is the length of the square element in the x-y plane. Linear (8-node isoparametric) and quadratic (20-node isoparametric) elements were nominated for the analyses. The planar refinement of mesh was carried out uniformly over several mesh densities ($\gamma = 1 - 58.82$) while no element subdivisions were carried out in the thickness direction. As depicted in Fig. 5a, the quadratic elements outperformed their linear counterparts and realised a quick convergence for mesh densities above 10. It was found that the linear elements required a higher mesh density to obtain an adequate h-type convergence. In this particular application, quadratic elements seemed to obtain a p-type convergence (Hellen and Becker, 2013) by moderate mesh densities. Moreover, the convergence rate seemed to be almost insensitive to the material contrast at different temperature extremes. In this step, the mesh density of 52.63 $^1/_\text{m}$ was selected to study the sensitivity of the quadratic elements in the thickness direction.
In the thickness direction, mesh densities ($\gamma = 200 - 2500$) were considered over which no considerable sensitivity was observed, see Fig. 5b. Finally, the planar mesh density of 52.63 $^1/_\text{m}$ and the through-thickness mesh density of 1250 $^1/_\text{m}$ was selected to carry out the parametric study.

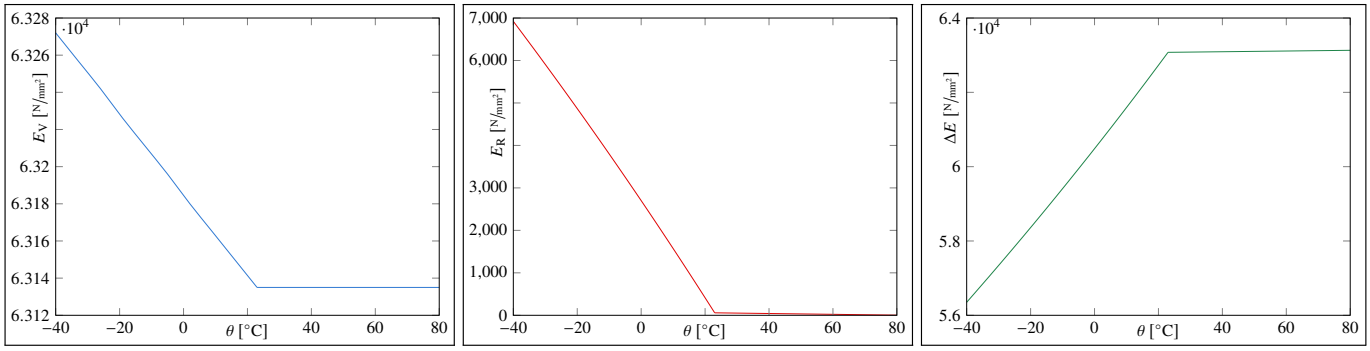

(a) (b) (c)

Fig. 6: Bounds of the elastic modulus of the composite behaviour at various temperatures: (a) Voigt bound, (b) Reuss bound, and (c) Voigt-Reuss difference.

4 Results and Discussion

4.1 Homogenisation

The bounds for a layered PV module are obtained using the Eqs. (3a) and (3b). Namely for a unit area of a PV module, the volumes of various layers are taken to calculate the volume fractions of skin and core layers. Consequently, the elastic moduli are obtained as follows:

$$E_{\mathrm{V}}(\theta) = {}^{1}/_{h}\,[2h_{\mathrm{s}}E_{\mathrm{s}} + h_{\mathrm{c}}E_{\mathrm{c}}(\theta)], \tag{14a}$$

$$E_{\mathrm{R}}(\theta) = \frac{hE_{\mathrm{c}}(\theta)E_{\mathrm{s}}}{2h_{\mathrm{s}}E_{\mathrm{c}}(\theta) + h_{\mathrm{c}}E_{\mathrm{s}}}. \tag{14b}$$

The graphical representation of these equations is presented in Fig. 6. It can be seen that as a result of the homogenisation process, the material properties along the principal directions are quite different. The degree of anisotropy for the elastic modulus could be simply represented by the $\Delta E = E_{\mathrm{V}} - E_{\mathrm{R}}$ difference (Aßmus et al., 2020). By increasing the temperature from −40 to +23°C, the bandwidth increases from $5.635 \cdot 10^4$ to $6.307 \cdot 10^4$ $^{\mathrm{N}}/_{\mathrm{mm}^2}$ and remains about the same value by further increasing the temperature, see Fig. 6c. Namely, at lower temperatures, the smaller bandwidth for elastic modulus indicates a better approximation for its range of possible values. However, from about the room temperature upwards there is only a slight increase in the bandwidth.
In terms of temperature-independent properties, the Voigt and Reuss bounds for Poisson's ratio are

$$\nu_{\mathrm{V}} = {}^{1}/_{h}\,[2h_{\mathrm{s}}\nu_{\mathrm{s}} + h_{\mathrm{c}}\nu_{\mathrm{c}}] = 0.3149, \tag{15a}$$

$$\nu_{\mathrm{R}} = \frac{h\nu_{\mathrm{c}}\nu_{\mathrm{s}}}{2h_{\mathrm{s}}\nu_{\mathrm{c}} + h_{\mathrm{c}}\nu_{\mathrm{s}}} = 0.3113, \tag{15b}$$

for which the parameters of Tab. 2 were used. The bandwidth of the Poisson's ratio estimates is $3.6 \cdot 10^{-3}$, which indicates a very good approximation. Similarly, the Voigt and Reuss bounds for effective mass density are obtained:

$$\rho_{\mathrm{V}} = {}^{1}/_{h}\,[2h_{\mathrm{s}}\rho_{\mathrm{s}} + h_{\mathrm{c}}\rho_{\mathrm{c}}] = 2287.83\ {}^{\mathrm{kg}}/_{\mathrm{m}^3}, \tag{16a}$$

$$\rho_{\mathrm{R}} = \frac{h\rho_{\mathrm{c}}\rho_{\mathrm{s}}}{2h_{\mathrm{s}}\rho_{\mathrm{c}} + h_{\mathrm{c}}\rho_{\mathrm{s}}} = 2035.61\ {}^{\mathrm{kg}}/_{\mathrm{m}^3}. \tag{16b}$$

The bandwidth of the mass density is $252.22\ {}^{\mathrm{kg}}/_{\mathrm{m}^3}$, which indicates a reasonable approximation.

4.2 Natural Frequencies and Mode Shapes

Mode shapes. The first nine mode shapes of the smeared composite is illustrated in Fig. 7a and the respective room-temperature computational results are depicted in Fig. 7b. It is evident that the proposed analytical procedure results in the same mode shapes as the computational model. In the FE model, the layers of PV module were modelled discretely and compared to the analytical procedure, the numerical effort does not seem to have any apparent advantages in detecting the mode shapes. Additionally, the Lanczos algorithm was used for the numerical solution of the eigenvalue problem, which is prone to produce spurious eigenvalues (Cullum and Willoughby, 2002). Thus, the analytical solution seems to be a better alternative in this sense. Nevertheless, the visual comparison of the mode shapes serves as a preliminary validation for both methods.

Natural frequencies. The Kirchhoff-Love plate theory for the homogenised medium was used to obtain the natural frequencies of the PV modules, see Tab. 4. Moreover, following a discrete modelling of the layers, the computational results are also presented in the same table. The obtained natural frequencies from both methods are related to their counterpart by Eq. (12). In order to develop a better understanding, two temperature extremes of −40°C and 80°C were considered along with the conventional room temperature of 23°C. All the values of the Voigt homogenisation demonstrated a negligible change at various temperatures. On the contrary, the Reuss bound showed a decrease by almost two orders of magnitude at all temperatures. This behaviour can be

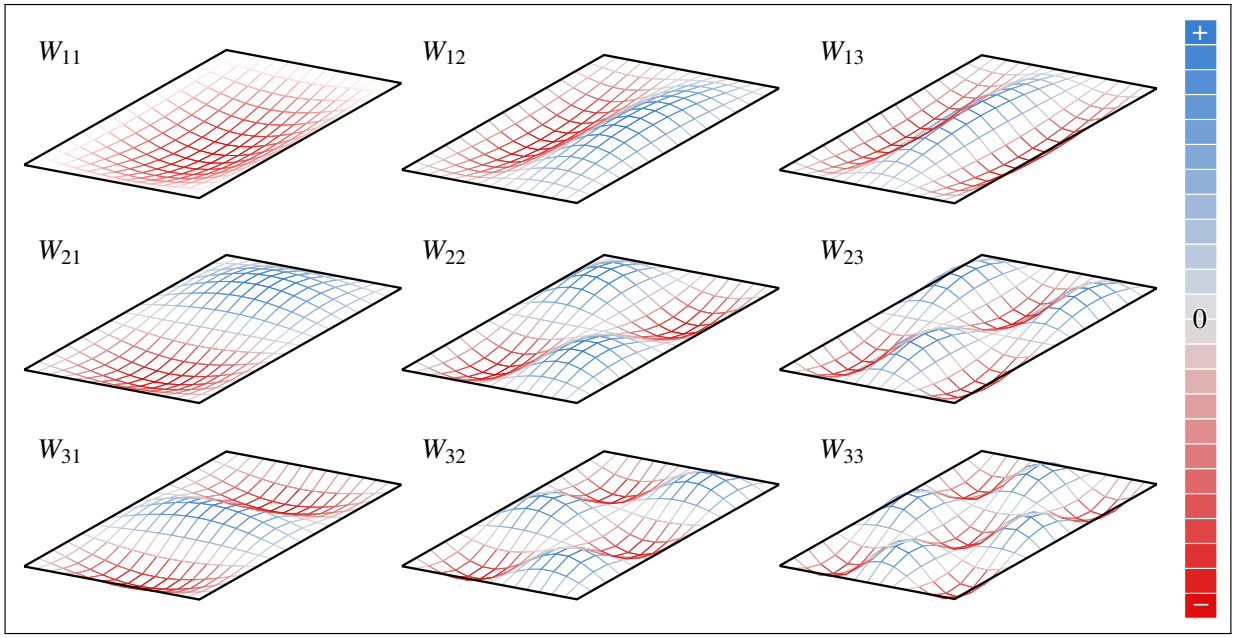

(a)

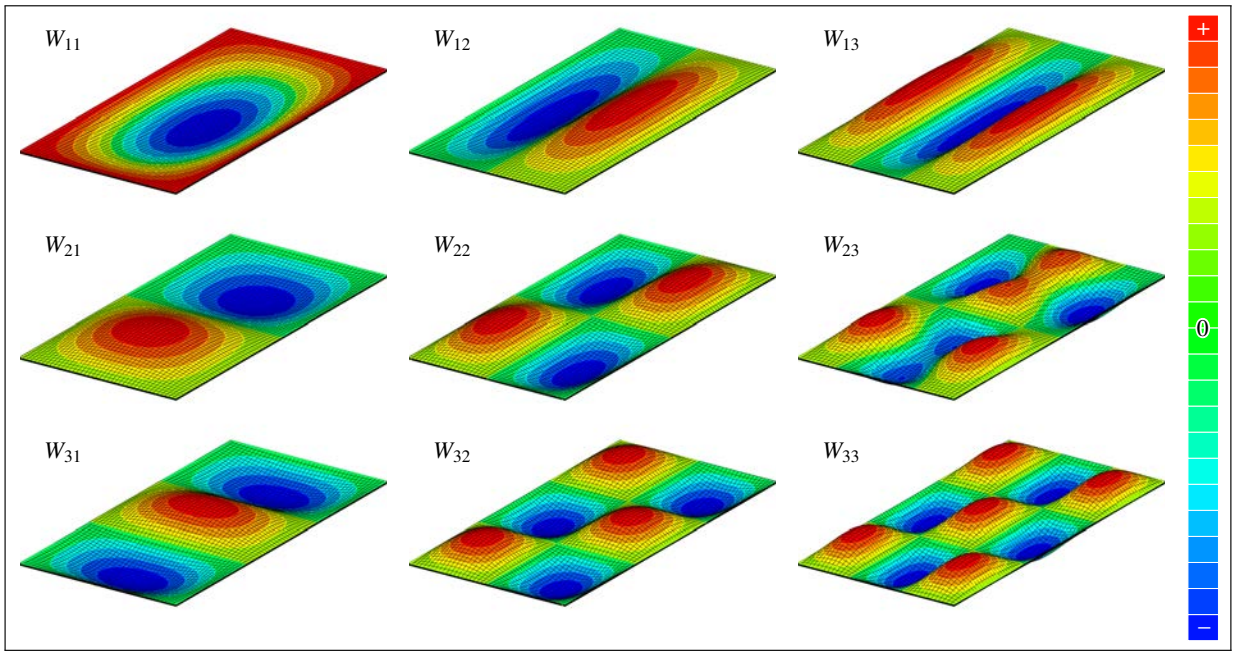

(b)

Fig. 7: Nine mode shapes of the photovoltaic module: (a) results of analytical solution, and (b) results of the computational solution at room temperature

attributed to the high contrast of mechanical properties, see Fig. 6c. Meanwhile, the computational results showed a decrease in the natural frequencies as the temperature increased up to +23°C where higher modes seemed to suffer a sharper decrease. Further increase in temperature resulted in additional decrease in the natural frequency, which became milder at higher frequencies. It can be concluded that while the Voigt bound seems to be insensitive to the material properties, the Reuss bound strongly reacts to the change of properties. The FE results followed the Voigt bound up to +15°C after which declined towards the Reuss bound. This behaviour can be attributed to the increase of the material contrast at higher temperatures.

Fundamental frequency. In Fig. 8, the results of the analytical solution and the computational model are illustrated for the fundamental frequency. As stated earlier, the Voigt bound seems to be insensitive to material contrast whereas the Reuss bound is more sensitive in that sense. The Voigt and Reuss bounds mark a wide range for the possible results. Namely, the computational results of the current study are in good agreement within the Reuss-Voigt range. More specifically, for the temperatures below 23°C, the Voigt bound matches the numerical results. By increasing the temperature, the computational results deviate from the Voigt bound. Nevertheless, the analytical bounds confirm that the results are within the acceptable range.

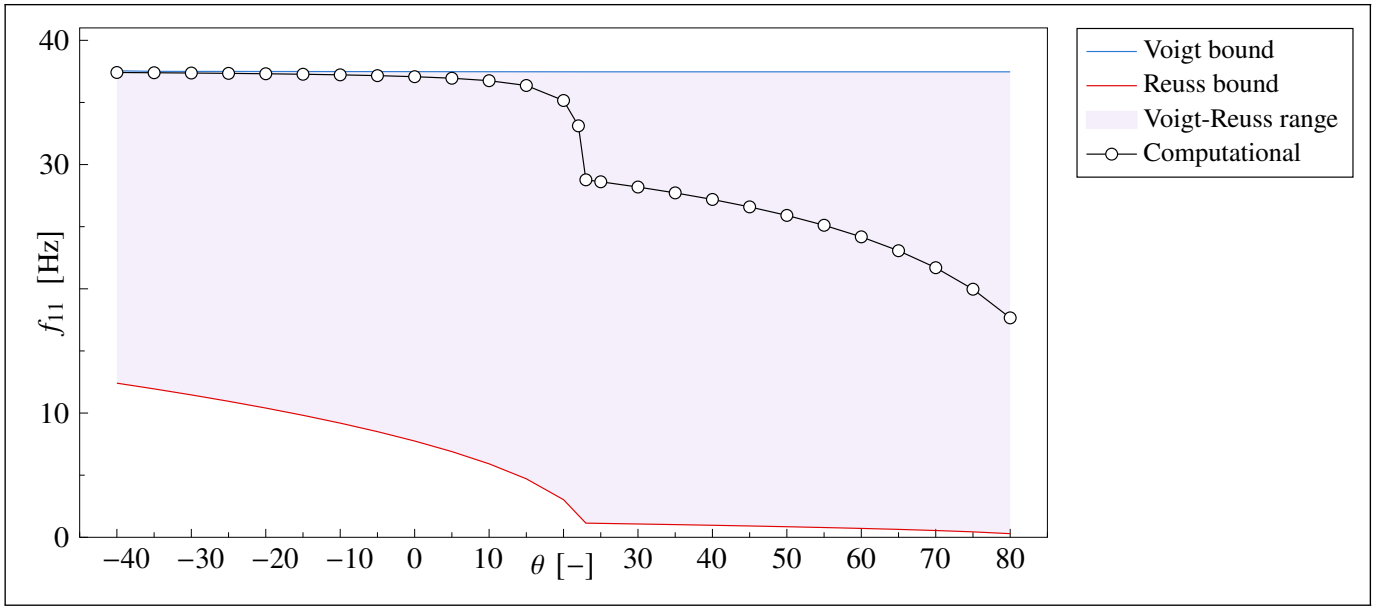

Fig. 8: Fundamental frequency results and the analytical bounds.

5 Final Remarks

Conclusion. The aim of the current study was to obtain a fast solution for the natural frequencies of PV modules. Although the analytical solution was not able to pinpoint the exact values of the fundamental frequencies over the whole temperature range, it provided a very good solution for the temperature range of −40 to 15°C. More specifically, the Voigt-Reuss range seemed to contain both experimental and computational results. In contrast, the provided computational model was able to provide more accurate results while demanding a sensible computational cost. The FE models were also able to mildly capture the effect of material contrast as a result of temperature change. The fundamental frequency of the examined PV module ranged between 17.66–37.41 Hz by decreasing the temperature. The value of 28.77 Hz was obtained for the room temperature fundamental frequency.
As many experimental efforts provide ranges for the natural frequencies rather than exact points, the introduced analytical method could be used to obtain a valid range for the results. On the other hand, if the computational procedure is preferred, the mesh sensitivity study recommends the use of quadratic elements and discrete modelling of the layers in order to alleviate the issue of high material property contrast.

Contributions. The major contributions of the current work can be listed as follows:

1. A new analytical procedure was suggested to obtain a range for the fundamental natural frequencies of PV modules or

Tab. 4: Obtained natural frequencies from the analytical solution combined with the Voigt (f^{V}), and Reuss (f^{R}) homogenisation schemes versus the results of the computational modelling (f^{C})

Homogenisation scheme	Mode (mn)								
	11	21	31	12	22	32	13	23	33
Analytical results									
$f^{\mathrm{V}}_{mn}(-40°\mathrm{C})$ [Hz]	37.55	60.08	97.64	127.68	150.21	187.76	277.89	300.42	337.97
$f^{\mathrm{V}}_{mn}(+23°\mathrm{C})$ [Hz]	37.46	59.94	97.41	127.38	149.86	187.32	277.24	299.72	337.18
$f^{\mathrm{V}}_{mn}(+80°\mathrm{C})$ [Hz]	37.46	59.94	97.41	127.38	149.86	187.32	277.24	299.72	337.18
$f^{\mathrm{R}}_{mn}(-40°\mathrm{C})$ [Hz]	12.41	19.85	32.25	42.18	49.62	62.028	91.80	99.25	111.65
$f^{\mathrm{R}}_{mn}(+23°\mathrm{C})$ [Hz]	1.14	1.82	2.96	3.88	4.56	5.69	8.43	9.11	10.26
$f^{\mathrm{R}}_{mn}(+80°\mathrm{C})$ [Hz]	0.29	0.47	0.76	0.99	1.17	1.46	2.16	2.34	2.63
Computational results									
$f^{\mathrm{C}}_{mn}(-40°\mathrm{C})$ [Hz]	37.41	59.49	96.58	126.97	148.38	184.34	273.67	294.45	329.34
$f^{\mathrm{C}}_{mn}(+23°\mathrm{C})$ [Hz]	28.77	42.12	62.77	78.46	88.81	106.07	146.88	156.37	172.37
$f^{\mathrm{C}}_{mn}(+80°\mathrm{C})$ [Hz]	17.66	26.93	42.26	54.52	63.65	78.87	115.60	124.70	139.89

possibly other anti-sandwich panels.

2. A clear computational procedure was described that can handle the high material contrast issue and produce more accurate results.
3. An analytical approximation was provided for the fundamental frequency of the PV modules in the temperature range of −40 to 15°C.

Outlook. The current study can be extended by conducting a parametric study to cover various sizes of commercial PV modules; considering the damping characteristics of the structure by considering the enclosing frame in the computational procedure or introducing a damping coefficient in the analytical procedure. Temperature-controlled experiments would also be beneficial for the validation of the extreme behaviours.

References

H. Altenbach. Analysis of homogeneous and non-homogeneous plates. In René de Borst and Tomasz Sadowski, editors, *Lecture notes on composite materials*, volume 154 of *Solid mechanics and its applications*, pages 1–36. Springer, Dordrecht, 2008. ISBN 978-1-4020-8771-4.

M. Aßmus. *Structural Mechanics of Anti-Sandwiches: An Introduction*. Springer Briefs in Continuum Mechanics. Springer, Cham, Switzerland, 2019. doi: 10.1007/978-3-030-04354-4.

M. Aßmus and M. Köhl. Experimental investigation of the mechanical behavior of photovoltaic modules at defined inflow conditions. *Journal of Photonics for Energy*, 2(1):1–11, 2012. doi: 10.1117/1.JPE.2.022002.

M. Aßmus, S. Jack, K.-A. Weiss, and M. Koehl. Measurement and simulation of vibrations of PVmodules induced by dynamic mechanical loads. *Progress in Photovoltaics: Research and Applications*, 19(6):688–694, 2011. doi: 10.1002/pip.1087.

M. Aßmus, K. Naumenko, and H. Altenbach. A multiscale projection approach for the coupled global–local structural analysis of photovoltaic modules. *Composite Structures*, 158:340–358, 2016. doi: 10.1016/j.compstruct.2016.09.036.

M. Aßmus, S. Bergmann, J. Eisenträger, K. Naumenko, and H. Altenbach. Consideration of non-uniform and non-orthogonal mechanical loads for structural analysis of photovoltaic composite structures. In H. Altenbach, R. V. Goldstein, and E. Murashkin, editors, *Mechanics for Materials and Technologies*, volume 46 of *Advanced structured materials*, pages 73–122. Springer International Publishing, Cham, 2017a. doi: 10.1007/978-3-319-56050-2_4.

M. Aßmus, S. Bergmann, K. Naumenko, and H. Altenbach. Mechanical behaviour of photovoltaic composite structures: A parameter study on the influence of geometric dimensions and material properties under static loading. *Composites Communications*, 5:23–26, 2017b. doi: 10.1016/j.coco.2017.06.003.

M. Aßmus, K. Naumenko, and H. Altenbach. Mechanical behaviour of photovoltaic composite structures: Influence of geometric dimensions and material properties on the eigenfrequencies of mechanical vibrations. *Composites Communications*, 6(-): 59–62, 2017c. doi: 10.1016/j.coco.2017.10.003.

M. Aßmus, R. Glüge, and H. Altenbach. On the analytical estimation for isotropic approximation of elastic properties applied to polycrystalline cubic silicon used at solar cells. *Technische Mechanik*, 40(2):120–133, 2020. doi: 10.24352/UB.OVGU-2020-020.

A. J. Beinert, P. Romer, M. Heinrich, M. Mittag, J. Aktaa, and H. Neuhaus. Thermomechanical evaluation of new PV module designs by fem simulations. In *36th European Photovoltaic Solar Energy Conference and Exhibition*, pages 783–788, 2019. doi: 10.4229/EUPVSEC20192019-4BO.11.1.

V. Birman. *Plate structures*, volume 178 of *Solid mechanics and its applications, 0925-0042*. Springer, Dordrecht, 2011. ISBN 9789400717145.

British Standards. Thin-film terrestrial photovoltaic (PV) modules - Design qualification and type approval: (IEC 61646:2008), 2008.

British Standards. Photovoltaic (PV) modules - Transportation testing: Part 1: Transportation and shipping of module package units (IEC 62759-1:2015), 2015.

British Standards. Photovoltaic (PV) modules - Cyclic (dynamic) mechanical load testing: (PD IEC/TS 62782:2016), 2016.

British Standards. Terrestrial photovoltaic (PV) modules - Design qualification and type approval: Part 1-2: Special requirements for testing of thin-film cadmium (IEC 61215-1-2:2016), 2017a.

British Standards. Terrestrial photovoltaic (PV) modules - Design qualification and type approval: Part 2: Test procedures (IEC 61215-2:2016), 2017b.

J. K. Cullum and R. A. Willoughby. *Lanczos algorithms for large symmetric eigenvalue computations*, volume 41 of *Classics in applied mathematics*. Society for Industrial and Applied Mathematics, Philadelphia, 2002. ISBN 0898715237.

W. Dallas, O. Polupan, and S. Ostapenko. Resonance ultrasonic vibrations for crack detection in photovoltaic silicon wafers. *Measurement Science and Technology*, 18(3):852–858, 2007. ISSN 0268-1242. doi: 10.1088/0957-0233/18/3/038.

S. Dietrich, M. Pander, M. Sander, S. H. Schulze, and M. Ebert. Mechanical and thermomechanical assessment of encapsulated solar cells by finite-element-simulation. In Neelkanth G. Dhere, John H. Wohlgemuth, and Kevin Lynn, editors, *Reliability of Photovoltaic Cells, Modules, Components, and Systems III*, volume 7773 of *SPIE Proceedings*, page 77730F. SPIE, 2010. doi: 10.1117/12.860661.

U. Eitner. *Thermomechanics of Photovoltaic Modules*. PhD-thesis, Martin-Luther-UniversitÃdt Halle-Wittenberg, 2011. URL http://nbn-resolving.de/urn:nbn:de:gbv:3:4-5812.

C. Ferrara and D. Philipp. Why do PV modules fail? *Energy Procedia*, 15:379–387, 2012. doi: 10.1016/j.egypro.2012.02.046.

T. Hellen and A. A. Becker. *Finite element analysis for engineers*. NAFEMS, Glasgow, 2013. ISBN 9781874376989.

Z. Javanbakht and A. Öchsner. *Advanced Finite Element Simulation with MSC Marc*. Springer International Publishing, Cham, 2017. ISBN 978-3-319-47667-4. doi: 10.1007/978-3-319-47668-1.

Z. Javanbakht and A. Öchsner. *Computational Statics Revision Course*. Springer International Publishing, Cham, 2018. ISBN 978-3-319-67461-2. doi: 10.1007/978-3-319-67462-9.

Z. Javanbakht, W. Hall, and A. Öchsner. The effect of partitioning on the clustering index of randomly-oriented fiber composites: a parametric study. *Defect and Diffusion Forum*, 380:232–241, 2017a. ISSN 1662-9507. doi: 10.4028/www.scientific.net/DDF.380.232.

Z. Javanbakht, W. Hall, and A. Öchsner. The effect of substrate bonding on characterization of thin elastic layers: A finite element study. *Materialwissenschaft und Werkstofftechnik*, 48(5):456–462, 2017b. ISSN 09335137. doi: 10.1002/mawe.201700035.

Z. Javanbakht, M. Aßmus, K. Naumenko, A. Öchsner, and H. Altenbach. On thermal strains and residual stresses in the linear theory of anti–sandwiches. *Journal of Applied Mathematics and Mechanics*, 99(8):1, 2019. doi: 10.1002/zamm.201900062.

Z. Javanbakht, W. Hall, and A. Öchsner. An element-wise scheme to analyse local mechanical anisotropy in fibre-reinforced composites. *Materials Science and Technology*, pages 1–13, 2020a. ISSN 0267-0836. doi: 10.1080/02670836.2020.1762296.

Z. Javanbakht, W. Hall, A. S. Virk, J. Summerscales, and A. Öchsner. Finite element analysis of natural fiber composites using a self-updating model. *Journal of Composite Materials*, page 002199832091282, 2020b. ISSN 0021-9983. doi: 10.1177/0021998320912822.

K. Kilikeviciene, J. Matijosius, A. Kilikevicius, M. Jurevicius, V. Makarskas, J. Caban, and A. Marczuk. Research of the energy losses of photovoltaic (pv) modules after hail simulation using a newly-created testbed. *Energies*, 12(23):4537, 2019. doi: 10.3390/en12234537.

A Kilikevicius, A Cereska, and K Kilikeviciene. Analysis of external dynamic loads influence to photovoltaic module structural performance. *Engineering Failure Analysis*, 66:445–454, 2016. ISSN 13506307. doi: 10.1016/j.engfailanal.2016.04.031.

G. Kirchhoff. Über das Gleichgewicht und die Bewegung einer elastischen Scheibe. *Journal für die reine und angewandte Mathematik (Crelles Journal)*, 1850(40):51–88, 1850. doi: 10.1515/crll.1850.40.51.

S. Koch, J. Kupke, D. Tornow, M. Schoppa, S. Krauter, and P. Grunow. Dynamic mechanical load tests on crystalline silicon modules. In *25th European Photovoltaic Solar Energy Conference and Exhibition*, pages 3998–4001, 2010. doi: 10.4229/25THEUPVSEC2010-4AV.3.11.

S. Köntges, M.and Kurtz, C. Packard, U. Jahn, K. A. Berger, and K. Kato. *Performance and reliability of photovoltaic systems: Subtask 3.2: Review of failures of photovoltaic modules : IEA PVPS task 13 : external final report IEA-PVPS*. International Energy Agency, Photovoltaic Power Systems Programme, Saint Ursen, Switzerland, 2014.

L. Meirovitch. *Fundamentals of vibrations*. McGraw-Hill, Boston, USA, 2001.

R. Mickiewicz, B. Li, D.M.J. Doble, T. Christian, J. Lloyd, A. Stokes, C. Völker, M. Winter, B. Ketola, A. Norris, and N. Shephard. Effect of encapsulation modulus on the response of PV modules to mechanical stress. In *26th European Photovoltaic Solar Energy Conference and Exhibition*, pages 3157–3161, 2011. doi: 10.4229/26THEUPVSEC2011-4CO.7.4.

K. Naumenko and V. A. Eremeyev. A layer-wise theory for laminated glass and photovoltaic panels. *Composite Structures*, 112: 283–291, 2014. doi: 10.1016/j.compstruct.2014.02.009.

S. Pingel, Y. Zemen, O. Frank, T. Geipel, and J. Berghold. Mechanical stability of solar cells within solar panels. In *24th European Photovoltaic Solar Energy Conference and Exhibition*, pages 3459–3463, 2009. doi: 10.4229/24thEUPVSEC2009-4AV.3.49.

J. N. Reddy. *Theory and analysis of elastic plates and shells*. CRC Press, Boca Raton, FL, 2nd ed. edition, 2006. ISBN 9780849384158.

F. Reil, J. Althaus, W. Vaassen, W. Herrmann, and K. Strohkendl. The effect of transportation impacts and dynamic load tests on the mechanical and electrical behaviour of crystalline PV modules. In *25th European Photovoltaic Solar Energy Conference and Exhibition*, pages 3989–3992, 2010. doi: 10.4229/25THEUPVSEC2010-4AV.3.9.

A. Reuss. Berechnung der Fließgrenze von Mischkristallen auf Grund der Plastizitätsbedingung für Einkristalle. *Zeitschrift für Angewandte Mathematik und Mechanik*, 9(1):49–58, 1929.

M. Sander, S. Dietrich, M. Pander, M. Ebert, and J. Bagdahn. Systematic investigation of cracks in encapsulated solar cells after mechanical loading. *Solar Energy Materials and Solar Cells*, 111:82–89, 2013. doi: 10.1016/j.solmat.2012.12.031.

A. C. Ugural. *Stresses in Beams, Plates, and Shells*. Taylor & Francis, 3rd edition, 2010.

N Visniakov, A Kilikevicius, J Novickij, A Grainys, and V Novickij. Low-cost experimental facility for evaluation of the effect of dynamic mechanical loads on photovoltaic modules. *Eksploatacja i Niezawodnosc - Maintenance and Reliability*, 17(3): 334–337, 2015. ISSN 15072711. doi: 10.17531/ein.2015.3.2.

W. Voigt. *Lehrbuch der Kristallphysik (mit Ausschluss der Kristalloptik)*. Teubner, Leipzig, 1910.

K-A Weiss, M Assmus, S Jack, and M Koehl. Measurement and simulation of dynamic mechanical loads on PV-modules. In Neelkanth G. Dhere, John H. Wohlgemuth, and Dan T. Ton, editors, *Reliability of Photovoltaic Cells, Modules, Components, and Systems II*, SPIE Proceedings, page 741203. SPIE, 2009. doi: 10.1117/12.824859.

J. Wohlgemuth. *Photovoltaic module reliability*. Wiley, Hoboken, NJ, USA, 2020. doi: 10.1002/9781119459019.